Surface & Coatings Technology 270 (2015) 266–271

Contents lists available at ScienceDirect

Surface & Coatings Technology

journal homepage: www.elsevier.com/locate/surfcoat

Depth distribution of martensite in plasma nitrided AISI H13 steel and its correlation to hardness

S.D. Jacobsen [a], R. Hinrichs [a,b], I.J.R. Baumvol [c], G. Castellano [d], M.A.Z. Vasconcellos [a,c,*]

[a] Programa de Pós-Graduação em Ciência dos Materiais, Universidade Federal do Rio Grande do Sul, Porto Alegre, RS, Brazil
[b] Instituto de Geociências, Universidade Federal do Rio Grande do Sul, Porto Alegre, RS, Brazil
[c] Instituto de Física, Universidade Federal do Rio Grande do Sul, Porto Alegre, RS, Brazil
[d] Facultad de Matemática, Astronomía y Física, Universidad Nacional de Córdoba, Argentina

ARTICLE INFO

Article history:
Received 7 January 2015
Accepted in revised form 23 February 2015
Available online 2 March 2015

Keywords:
Plasma nitriding
AISI H13
Hardness
Phase distribution

ABSTRACT

The depth distributions of hardness, nitrogen, and crystallographic phases in the diffusion zone of plasma nitrided AISI H13 steel were determined by microindentation, electron microprobe, grazing incidence X-ray diffraction, and conversion electron Mössbauer spectroscopy. For the phase analysis, successively new surfaces were exposed by means of controlled mechanical layer removal. In the diffusion zone, the nitrogen concentration decreases monotonously, while the hardness profile exhibits two distinct regions, one where hardness is roughly constant and another where it decreases to bulk values. Thus, in the case investigated here, the common sense of a linear dependence of hardness on the N concentration does not apply in both regions, but only in the second one. This behavior is discussed in terms of the above mentioned physico-chemical properties.

1. Introduction

Plasma nitriding is a surface engineering technology widely used to improve the tribological and mechanical properties of steel surfaces. In this process, the diffusion of nitrogen species from the plasma leads to the formation of nitrogenous phases in the near surface region [1–3].

The AISI H13 is a commonly used steel in hot working applications [4] and, next to other surface treatments [5], plasma nitriding is employed to increase its hardness and wear resistance. During this treatment, two different layers can be formed: the compound layer and the diffusion zone. The compound layer, which is the outermost one, usually consists of iron nitrides such as ε-$Fe_{2-3}N$, γ′-Fe_4N, or a mixture of these phases [6,7]. Below is the diffusion zone, described by some authors as a cubic ferrite structure (α-Fe) with dissolved nitrogen [8], while other authors refer to this region as containing tetragonal nitrogen-martensite, α′-Fe(N) [2,7]. The importance of the so called "excess" nitrogen in the diffusion zone has been reported, attributing its incorporation to the formation of nanoprecipitates of alloying element-nitrides, nitrogen absorption in the interfaces between the precipitates and the matrix, and interstitial nitrogen in the iron lattice [9–11].

Several authors have investigated the interdependence of hardness and nitrogen content in the compound layer and/or in the diffusion zone, and many describe a linear relationship between them [10–17], while others do not observe any correlation [18]. In the compound layer a linear dependence was observed [14,17] and was mostly attributed to the saturation with nitrogen, with the formation of ε-$Fe_{2-3}N$ and γ′-Fe_4N. The hardness in this case is determined by the proportion of these phases. In the diffusion zone a linear correlation between hardness and nitrogen concentration was reported [10,11,15]. Hardness behavior at different depths was attributed partly to the formation of CrN precipitates [15], even if only a low fraction of this phase was formed.

Major attention has been dedicated to the role of nitride precipitates/nanoprecipitates on the improvement of the mechanical properties after nitriding. Few discussions are focused on the structural modification of the ferritic/martensitic matrix in the diffusion zone as a consequence of the excess of nitrogen observed in this region. Although nitrogen concentrations up to 12 at.% have been found in the diffusion zone of low temperature nitrided AISI H13 steel, the linear correlation between hardness and nitrogen concentration was only observed below 7 at.% nitrogen [11]. Another study in the same steel showed a constant behavior of the hardness along the diffusion zone and stated that no simple dependence on the content of precipitates of metallic nitrides can explain this observation [15]. These results point out the need to investigate the relation between phases and mechanical properties in the diffusion zone of nitrided steel.

We report here on the determination of the hardness depth profile in AISI H13 steel plasma nitrided in a specific condition, as well as on the depth distributions of nitrogen and crystallographic phases formed in the diffusion zone, investigating the relationships between these parameters. The nitrogen profile and the hardness, measured on the

* Corresponding author at: Av. Bento Gonçalves 9500, p.o. box 15051, 91501-970 Porto Alegre, RS, Brazil. Tel.: +55 51 3308 6539.
E-mail address: marcos@if.ufrgs.br (M.A.Z. Vasconcellos).

http://dx.doi.org/10.1016/j.surfcoat.2015.02.046
0257-8972/

Table 1
Chemical composition of the AISI H13 steel in wt.%.

C	Mn	Si	P	Mo	Cr	V	Fe
0.4	0.35	1.0	1.0	1.4	5.15	–	Balance

cross section of the sample, were compared with the depth distribution of phases, as determined by two complementary, surface-sensitive techniques, namely grazing incidence X-ray diffraction (GIXRD) and conversion electron Mössbauer spectroscopy (CEMS). As these techniques probe only to a 1 μm depth approximately, it was necessary to sequentially expose surfaces by controlled mechanical layer removal. The chosen nitriding condition produced a thick diffusion layer that allowed the removal of more than a dozen slices and phase analysis to a depth of several tens of μm.

2. Experimental

Samples were cut from AISI H13 steel rods and machined into discs with 18 mm diameter and 5 mm thickness. The samples were ground, austenitized at 1020 °C for 30 min, quenched in oil, tempered for 2 h at 600 °C, metallographically polished, degreased with ether, and then ultrasonically cleaned in acetone for 30 min. The nominal chemical composition of the AISI H13 steel is shown in Table 1.

The glow-discharge chamber was pumped down to a base pressure of 3 Pa. The samples were plasma-etched in argon at 800 Pa, 350 °C for 30 min. Nitriding was performed for 5 h in a 80%-N_2:20%-H_2 gas mixture, flow rate of 20 sccm, and pressure of 800 Pa. To maintain the sample temperature at 450 °C, the voltage was adjusted to 347 V and the current to 287 mA. The sample holder was designed such as to decrease edge effects during the treatment, allowing the insertion of three samples in circular troughs, leveling the surfaces exposed to the plasma.

After the nitriding process, the samples were prepared for characterization in two ways: i) a laborious procedure removing sequentially fourteen thin layers via mechanical polishing starting at the nitrided sample surface, to analyze each one of the newly exposed surfaces with GIXRD and CEMS for phase identification; ii) polished cross sections for hardness profiles measured in a dynamic ultra-microhardness tester (Shimadzu DUH211S), and for nitrogen concentration analysis with an electron microprobe analyzer. After Nital etching, images of the cross section were obtained in a scanning electron microscope (Jeol LV5800).

The parallelism control of the grinding procedure that removed layers of few micrometers was done with the aid of a previous indentation pattern on three points of the sample perimeter. The patterns were observed in an optical microscope (Zeiss Axiotech) and the thickness of each removed layer was calculated by geometrical means.

GIXRD (Shimadzu XRD 6000) was performed with 2° incidence angle, enabling phase identification of the uppermost 600 nm of the sample. The GIXRD patterns were interpreted by comparison with the cards of the Powder Diffraction File™ (PDF) from the International Center for Diffraction Data (ICDD®). Rietveld analysis was performed with the FullProf Suite software [19].

CEMS performed in backscattering geometry is an especially adequate tool to identify iron-based phases in the 100 nm layer below the surface. The spectra were acquired using a ^{57}Co source in Rh matrix and a proportional counter with He-5%:CH_4 flow. The data were fitted with *WinNormos* on IGOR® software, using hyperfine parameters from the literature as initial values. Isomer shifts are presented relative to α-Fe.

Hardness and elastic modulus profiles were determined on the cross section in a microhardness tester (Shimadzu DUH 211 S) with a Berkovich indenter using a peak load of 100 mN in each cycle [20]. Mean hardness and standard deviation were obtained from ten measurements at each depth.

The nitrogen concentration was determined on the same cross section with an electron microprobe (Jeol JXA 8230), using a 15 keV electron beam with 10 nA, in steps of 3 μm, counting the N-Kα x-rays with the aid of a synthetic analyzing crystal, and quantifying the results with ZAF matrix corrections [21].

3. Results and discussion

Nitrogen concentration and hardness profiles are shown in Fig. 1. The relative uncertainties for nitrogen concentration are estimated to be around ±5%. The vertical scales were adjusted to show the match of the two profiles in the third region.

Three regions can be discriminated in the profiles: ① from the surface down to 8 μm; ② from 8 μm to 45 μm, and ③ from 45 μm to 80 μm. In region ①, with nitrogen concentration above 10 at.%, a compound layer was observed by SEM and confirmed by GIXRD. In region ② the nitrogen content decreased from 11 to 6 at.%, while hardness was roughly constant. In region ③, nitrogen content and hardness show the same trend with depth, decaying to bulk levels below 80 μm.

The last two regions comprise the diffusion layer, where it is generally observed that hardness correlates linearly with the nitrogen concentration [9,12–14]. This was also observed for region ③ of the present work, where N concentration is below 6 at.%. In this concentration range the curves superpose well [11,12,16]. However, in region ② the nitrogen concentration and hardness do not correlate.

In order to clarify the origin of the deviation from linear relationship between nitrogen content and hardness in region ②, the set of diffraction patterns obtained with the first sample preparation procedure outlined above, is shown in Fig. 2, starting at the surface down to the

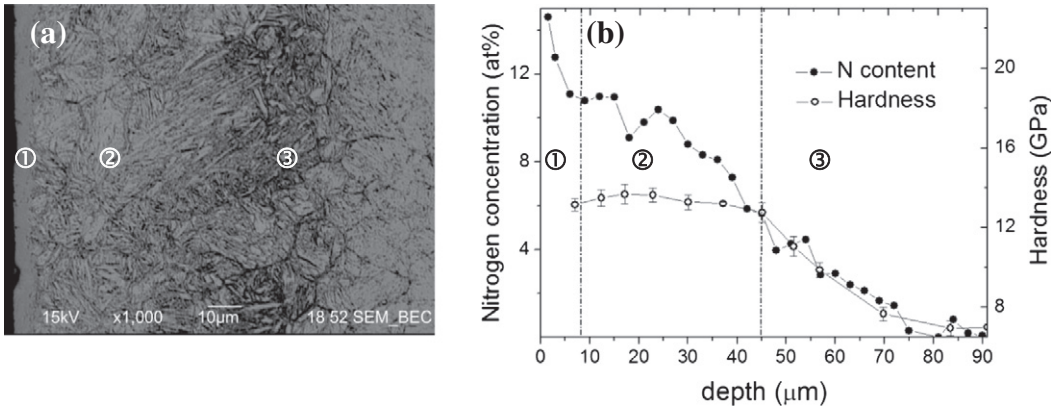

Fig. 1. (a) SEM micrograph of the compound layer ① and the diffusion layers (② and ③); (b) depth profiles of nitrogen concentration (filled symbols) and hardness (open symbols) obtained of the same region.

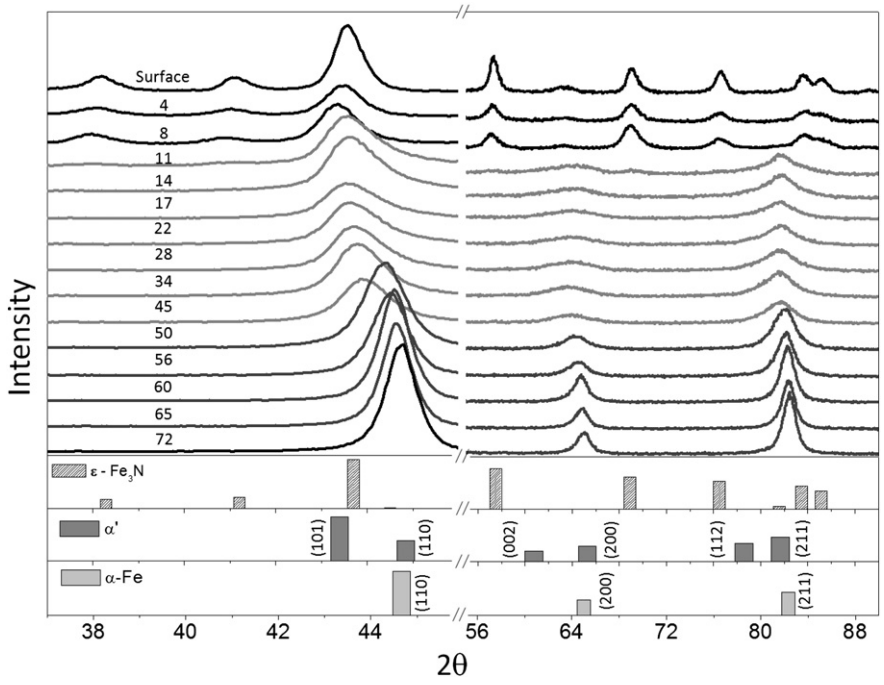

Fig. 2. GIXRD patterns obtained with 2° incidence (depth below original surface is indicated). The histograms show the peak positions of the ε-Fe_3N (PDF 73-2101), α′-Fe(N) with 5 at.% N (PDF 75-2140), and α-Fe (PDF 87-0721).

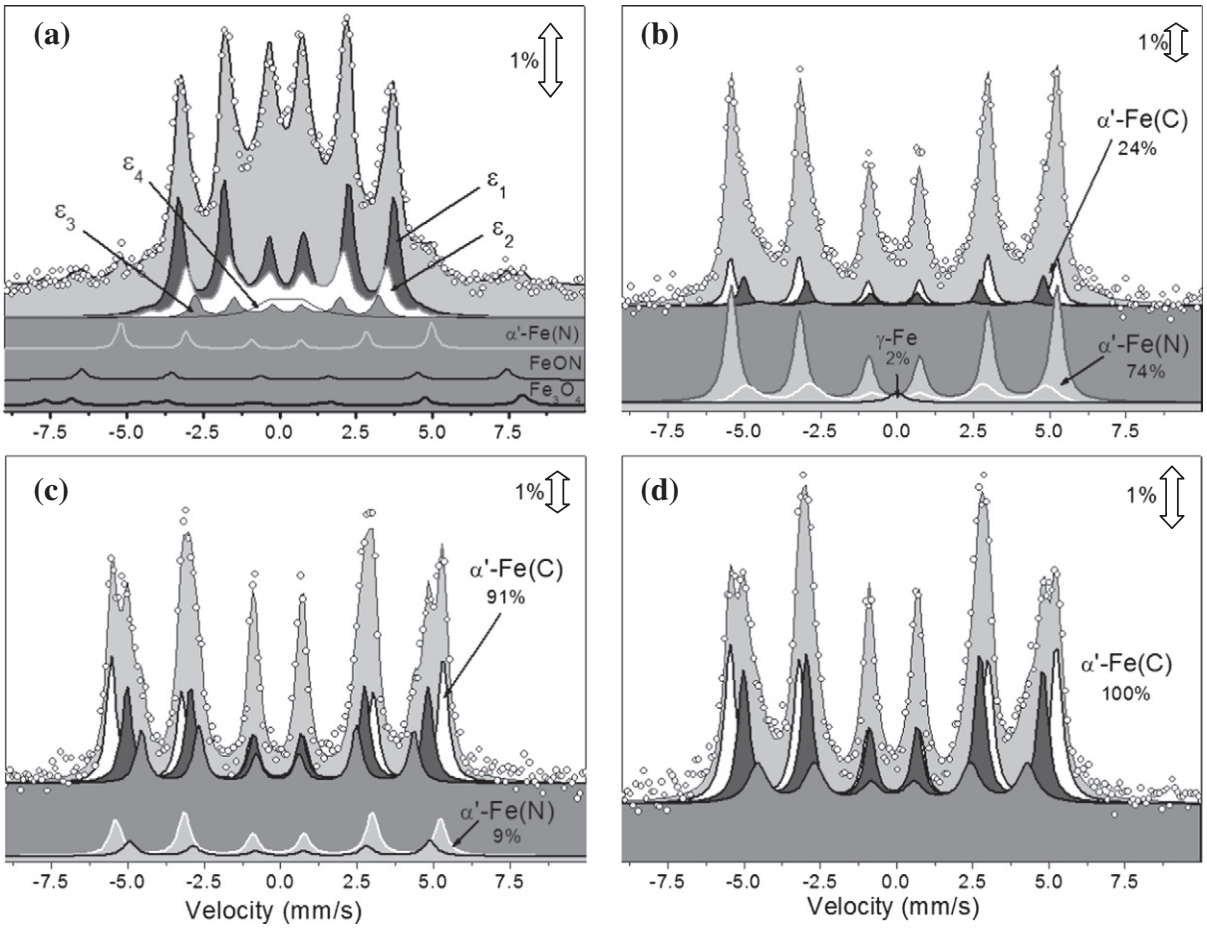

Fig. 3. CEMS spectra from (a) the surface layer (region ①), (b) the layer exposed after the removal of 22 μm (region ②), (c) the layer at 65 μm depth (region ③), and (d) bulk of AISI H13 steel. The phases identified in (a) are ε-$Fe_{2-3}N$, nitrogen martensite α′-Fe(N), iron oxy-nitride FeON, and magnetite Fe_3O_4; in (b) and (c) carbon martensite α′-Fe(C) and nitrogen martensite α′-Fe(N) plus vestigial austenite γ-Fe in (b), and in (d) only carbon-martensite α′-Fe(C). The white double arrow in the upper right corner of each spectrum indicates 1% effect.

Table 2
Hyperfine parameters and relative areas of the CEMS spectra of Fig. 3, for phases at the surface (region ①), at 22 μm (region ②) and at 65 μm (region ③). References of the parameters are [24–27].

Phase		H (T)	IS (mm/s)	QS (mm/s)	Relative area (%)			
					Surface ①	22 μm ②	65 μm ③	Bulk
ε_1	ε-Fe_3N	28.57	0.21	0	41			
		21.83	0.33	0				
		7.0	–	0				
ε_2	ε-$Fe_{2,67}$ N	27.3	0.26	0	34			
		20.4	0.34	0				
		9.95	0.4	0				
ε_3	ε-$Fe_{2,47}$ N	18.6	0.35	0	6			
		8.4	0.41	0				
ε_4	ε-Fe_2N	–	0.42	0.31	12			
Fe_3O_4		45.67	0.66	0	2			
		48.76	0.28	0				
FeON		43.17	0.58	0	2			
α′-Fe(N)		33.1	−0.04	0	3	74	9	
		30.8	0.08	0				
α′-Fe(C)		33.2	0.01	0		24	91	
		30.4	0.00	0				100
		27.5	−0.03	0				
γ-Fe		–	−0.03	0		2		

different indicated depths (in micrometers). Since all removed layers were thicker than the analyzed depth in each pattern, the method avoids the interference of outer layers that occurs, for instance, when the surface is probed with varying incidence angle GIXRD.

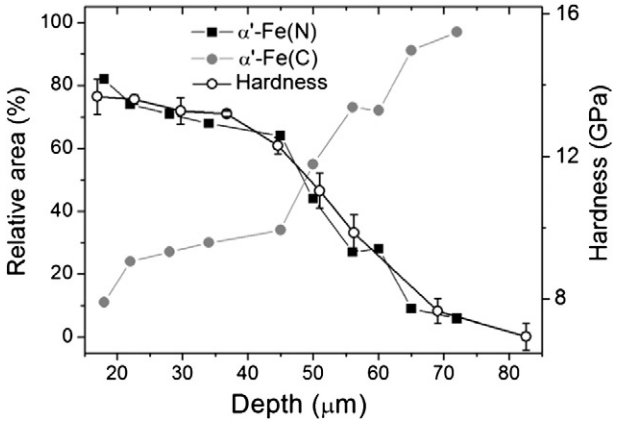

Fig. 4. Depth distribution of nitrogen martensite (full squares), carbon-martensite (full circles), and hardness (open circles).

Three groups of patterns can be distinguished: from the surface down to 8 μm depth, from 11 μm to 45 μm, and deeper than 50 μm. In the group closest to the sample surface, the patterns were fully consistent with the ε-phase (PDF 73-2101), identifying the compound layer. In the second group the pattern was consistent with the presence of α′-Fe(N) (PDF 75-2140). In this group the peak broadening and the shift to the left of the peaks between 43 and 45° were attributed to a variable content of nitrogen that induces progressive tetragonalization of the lattice, increasing the c-axis of the formerly cubic cell and slightly reducing the a-parameter of the base [22,23]. When the c/a ratio of the unit cell increases, the (101) peak of martensite displaces to lower angles, while the (110) peak remains in the same position. This trend of the peaks in the diffraction patterns of the diffusion zone was also observed by other authors [11]. Below 50 μm, first inspection indicated the presence of α-iron (PDF 87-0721), and the patterns were compatible with the steel bulk. The depth at which the GIXRD patterns change corresponds to the same boundaries as regions ①, ②, and ③ observed in Fig. 1.

CEMS spectra were obtained from all the surfaces analyzed with GIXRD. The spectra can be grouped in the same manner as the GIXRD patterns. For the sake of clarity only one representative spectrum of each group is shown in Fig. 3. Region ① is represented by the spectrum of the surface, region ② by the spectrum of 22 μm, and region ③ by the spectrum of 65 μm. For comparison a spectrum from the bulk is shown as well.

The CEMS spectrum from the near surface region of the nitrided sample presented in Fig. 3(a), shows the dominant presence of the ε-phase, in agreement with the diffraction patterns from this region. However, CEMS can recognize the different stoichiometries of this phase [24], identified as ε_1-ε_4, numbered according to rising nitrogen content. The sextet due to the phase ε-$Fe_{3.2}N$ (ε_1) shows the highest relative area, followed by ε-$Fe_{2.67}N$ (ε_2), ε-$Fe_{2.47}N$ (ε_3), and ε-Fe_2N (ε_4). Minor contributions of magnetite (Fe_3O_4) [25], iron oxy-nitride (FeON) [26], and nitrogen-martensite (α′-Fe(N)) are observed as well. The spectrum in Fig. 3(b) represents the diffusion zone, with more nitrogen-martensite than carbon-martensite and vestigial austenite [25], while in Fig. 3(c) the spectrum shows more carbon- than nitrogen-martensite. Fig. 3(d) displays the spectrum of the bulk H13 steel, containing only carbon-martensite.

The GIXRD pattern of the bulk steel appeared compatible with a ferrite diffraction pattern with slightly broadened peaks, and it was expected that a single iron sextet with hyperfine field of 33 T would fit the CEMS spectrum. However, two additional sextets with hyperfine fields 30.4 T and 27.4 T had to be used, as for carbon containing martensite [27]. These three sets of hyperfine parameters are related to the presence of (at least) three distinct sites of iron in the carbon-martensite. The first field is equivalent to the ferrite field and is due to the iron atoms far from any interstitial carbon atom. The hyperfine fields with 30.4 T and 27.4 T are related to structure modifications induced by

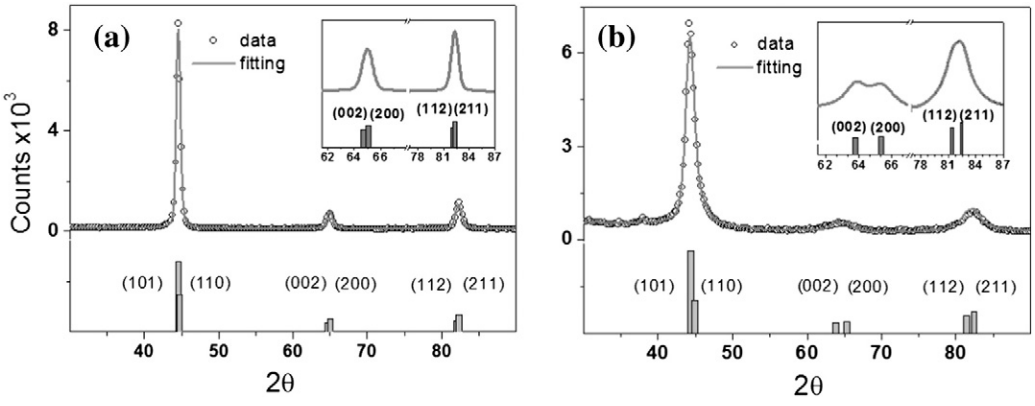

Fig. 5. Rietveld refinement of the diffraction patterns from (a) the AISI H13 bulk, (b) the layer at 22 μm depth. The insets show expanded views of the patterns between 62 and 87° (2θ).

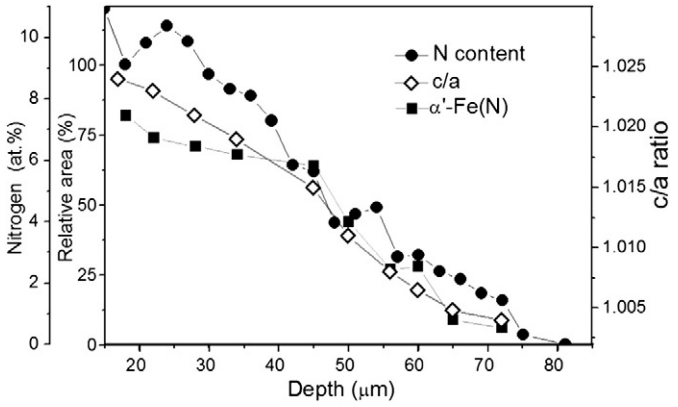

Fig. 6. Depth distribution of nitrogen concentration (filled circles), *c*/*a* ratio (open symbols) and percentage of α′-Fe(N) (filled squares).

carbon atoms in octahedral and tetrahedral interstices [27,28]. The spectrum in Fig. 3(b) corresponds to the intermediate region, and was adjusted with components from carbon-martensite, nitrogen-martensite and a minor contribution of carbon-austenite. The fitting of the nitrogen-martensite used the parameters proposed by Kopcewicz [24]: a sextet from α-iron and one additional sextet with a hyperfine field of 30.8 T. Since the latter sextet presents very broad lines for Mössbauer standards (linewidth of 1.5 mm/s), it could be argued that it would be compatible as well with the superposition of sextets with thinner lines due to multiple hyperfine fields [24]. This would reveal better the analogy with carbon-martensite, because nitrogen atoms can occupy equivalent interstitial sites as carbon in the iron structure.

Table 2 shows the fitting parameters of the Mössbauer spectra and the area fractions of the phases present in the surface layer, at 22 and at 65 μm depth, and in the steel bulk. It is noteworthy that the relative area of each spectrum is calculated with respect to the total of iron based phases, because CEMS is insensitive to e.g. CrN.

The relative areas in Table 2 provide an indication of the amount of each phase. The conversion of spectral area fractions to phase concentration is a difficult task, requiring corrections for finite thickness, phase composition, and recoil-free fraction effects for each phase [29]. For practical purposes, the behavior of the depth distribution of phase content can be qualitatively evaluated using the relative area without these corrections, since the concentrations of carbon or nitrogen in the diffusion zone only represent a minor difference from the composition of the steel bulk.

Fig. 4 shows the relative areas of carbon- and nitrogen-martensites for all exposed surfaces of the diffusion layer, as well as the hardness, measured in the same regions of the cross section.

When the relative amount of carbon-martensite and nitrogen-martensite is compared along the depth profile, it can be seen that the incoming nitrogen pushes the carbon deeper into the sample. This is an effect that has been observed before in both austenitic [30,31] and martensitic steels [32]. Although recurrently observed, we could not find a satisfactory explanation for this effect in the literature. Nevertheless, one can suppose that the propagating nitrogen front might well dislodge the carbon atoms, pushing them deeper into the sample. The H13 steel is not fully saturated in interstitial carbon and therefore it is possible to envision its migration via unoccupied octahedral sites in the matrix.

When the amount of nitrogen-martensite in the diffusion zone is compared to hardness, it can be seen that they correlate well in the whole range. Recalling Fig. 1(b), which depicts nitrogen content and hardness in the same region, a linear correlation between the nitrogen profile and hardness is observed between 80 and 45 μm depth. However, in the region between 17 and 45 μm, where the hardness shows a 10% decrease, the nitrogen content is reduced by almost 50% (Fig. 1b). In order to evaluate if the observed N-excess can be associated with its incorporation into the lattice of martensite, the GIXRD patterns were refined with Rietveld analysis.

Fig. 5 shows the GIXRD patterns and the Rietveld refinement from the steel bulk (in Fig. 5(a)), and the region with N-excess (in Fig. 5(b)).

Fig. 5(a) shows that the bulk steel contains enough carbon to produce a martensite structure, with a *c*/*a* ratio around 1.004. The small deviation from the cubic structure explains why this pattern is often interpreted as ferrite. In Fig. 5(b) it becomes clear that the broadening observed in region 2 of Fig. 2 corresponds to the relative displacement of the planes (101)/(110), (002)/(200), and (112)/(211). This is due to the increasing distortion of the tetragonal structure with the insertion of nitrogen, represented by the *c*/*a* ratio, as can be seen in the splitting of the peaks in Fig. 5(b).

Fig. 6 shows the *c*/*a* ratio determined from the Rietveld refinements, the nitrogen concentration, and the α′-Fe(N) phase content against the depth of the nitrided sample.

It can be seen that the *c*/*a* ratio is higher in the region where the nitrogen-martensite content is almost constant, explaining the increase of N-content as a result of the higher insertion of nitrogen into the martensite structure. Indeed, it has been proposed that the increase of the *c*/*a* ratio is roughly proportional to the atomic nitrogen concentration [22].

The correlations of hardness with α′-Fe(N) content and N-content are summarized in Fig. 7.

It can be seen that the linear relationship between hardness and the α′-Fe(N) content holds for the whole diffusion zone (Fig. 7(a)), while the linear relationship between hardness and nitrogen concentration is only valid below 6 at.% (Fig. 7(b)).

4. Conclusions

The correlation of the hardness profile in the diffusion zone of plasma nitrided steel with the profiles of nitrogen concentration and of nitrogen-martensite (α′-Fe(N)) content was made in a specific

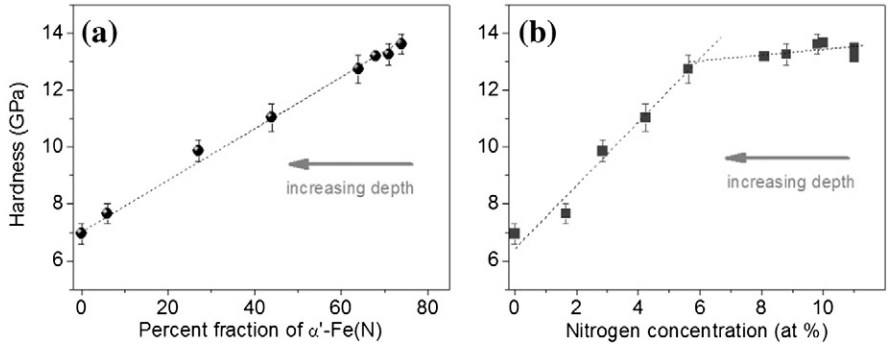

Fig. 7. Hardness plotted against (a) percent fraction α′-Fe(N) (circles) and (b) nitrogen concentration (squares). The dotted lines are only to guide the eyes.

plasma nitriding condition, with a specific steel (AISI H13). The hardness profile presented two distinct regions, one where the hardness is roughly constant and another where it decreases to the hardness of the bulk. The hardness profile was found to scale well with the N concentration in the second region, below 6 at.% N. Above this concentration, there was no correlation between the hardness and the N values, as the N concentration continued to increase towards the surface, while the hardness profile presented a very slow growth, almost a plateau. In the nitriding conditions of the present study, on the other hand, the hardness profile was seen to be proportional to the depth distribution of nitrogen-martensite in the whole N-concentration range, evidencing a correlation between the amount of nitrogen-martensite with hardness. The excess of N in the diffusion layer next to the compound layer, is partly attributed to the increase of nitrogen inside the martensitic unit cells. In this region, the *c*/*a* ratio increases, explaining the increase of N-content as a result of the higher insertion of nitrogen into the martensite structure, while the volumetric amount of martensite is constant, as is the hardness. Other mechanisms of nitrogen uptake, as alloying-element nitrides forming nano-precipitates are not excluded, but do not seem to control the hardness behavior in this case, which is consistent with the martensite content in the whole diffusion layer.

Acknowledgments

The authors acknowledge financial support from the Brazilian funding agencies CAPES (PPCP 014/2011), CNPq (479940/2010-0), and APERGS (1012175) and from the Argentinean SPU/Ministerio de Educación. S. D. J thanks the grant from Instituto Nacional de Engenharia de Superfícies/INCT (554336/2010-3).

References

[1] H. Michel, T. Czerwiec, M. Gantois, D. Ablitzer, A. Ricard, Surf. Coat. Technol. 72 (1995) 103. http://dx.doi.org/10.1016/0257-8972(94)02339-5.
[2] M.B. Karamış, K. Yıldızlı, G.Ç. Aydın, Tribol. Int. 51 (2012) 18. http://dx.doi.org/10.1016/j.triboint.2012.02.005.
[3] J. Walkowicz, Surf. Coat. Technol. 174 (2003) 1211. http://dx.doi.org/10.1016/S0257-8972Ž03.00656-X.
[4] M.B. Karamış, Wear 150 (1991) 331. http://dx.doi.org/10.1016/0043-1648(91)90327-Q.
[5] A.L. Yerokhin, X. Nie, A. Leyland, A. Matthews, S.J. Dowey, Surf. Coat. Technol. 122 (1999) 73. http://dx.doi.org/10.1016/S0257-8972(99)00441-7.
[6] M.R. Cruz, L. Nachez, B.J. Gomez, L. Nosei, J.N. Feugeas, M.H. Staia, Surf. Eng. 22 (2006) 359. http://dx.doi.org/10.1179/174329406X126663.
[7] R.L.O. Basso, R.J. Candal, C.A. Figueroa, D. Wisnivesky, F. Alvarez, Surf. Coat. Technol. 203 (2009) 1293. http://dx.doi.org/10.1016/j.surfcoat.2008.10.006.
[8] L.F. Zagonel, E.J. Mittemeijer, F. Alvarez, Mater. Sci. Technol. 25 (2009) 726. http://dx.doi.org/10.1179/174328408X332780.
[9] S.S. Hosmani, R.E. Schacherl, E.J. Mittemeijer, Acta Mater. 54 (2006) 2783. http://dx.doi.org/10.1016/j.actamat.2006.02.017.
[10] M. Sennour, C. Jacq, C. Esnouf, J. Mater. Sci 39 (2004) 4533. http://dx.doi.org/10.1023/B:JMSC.0000034147.58126.f8.
[11] L.F. Zagonel, J. Bettini, R.L.O. Basso, P. Paredez, H. Pinto, C.M. Lepienski, F. Alvarez, Surf. Coat. Technol. 207 (2012) 72. http://dx.doi.org/10.1016/j.surfcoat.2012.05.081.
[12] I. Alphonsa, A. Chainani, P.M. Raole, B. Ganguli, P.I. John, Surf. Coat. Technol. 150 (2002) 263. http://dx.doi.org/10.1016/S0257-8972(01)01536-5.
[13] L.H. Corredor, B. Chornik, G. Ishizaki, Scr. Metall. 15 (1981) 195. http://dx.doi.org/10.1016/0036-9748(81)90328-8.
[14] E.A. Ochoa, C.A. Figueroa, F. Alvarez, Surf. Coat. Technol. 200 (2005) 2165. http://dx.doi.org/10.1016/j.surfcoat.2004.09.004.
[15] L.F. Zagonel, C.A. Figueroa, R. Droppa Jr., F. Alvarez, Surf. Coat. Technol. 201 (2006) 452. http://dx.doi.org/10.1016/j.surfcoat.2005.11.137.
[16] R.L.O. Basso, C.A. Figueroa, L.F. Zagonel, H.O. Pastore, D. Wisnivesky, F. Alvarez, Plasma Process. Polym. 4 (2007) 728. http://dx.doi.org/10.1002/ppap.200731806.
[17] E.A. Ochoa, D. Wisnivesky, T. Minea, M. Ganciu, C. Tauziede, P. Chapon, F. Alvarez, Surf. Coat. Technol. 203 (2009) 1457. http://dx.doi.org/10.1016/j.surfcoat.2008.11.025.
[18] M. Asgari, A. Barnoush, R. Johnsen, R. Hoel, Tribol. Int. 61 (2013) 109. http://dx.doi.org/10.1016/j.triboint.2012.12.004.
[19] J. Rodriguez-Carvajal, Physica B 192 (1993) 55. http://dx.doi.org/10.1016/0921-4526(93)90108-I.
[20] W.C. Oliver, G.M. Pharr, J. Mater. Res. 7 (1992) 1564. http://dx.doi.org/10.1557/JMR.1992.1564.
[21] J.I. Goldstein, D.E. Newbury, P. Echlin, D.C. Joy, C.E. Lyman, E. Lifshin, L. Sawyer, J.R. Michael, Scanning Electron Microscopy and X-ray Microanalysis, Third edition Springer, New York, 2003.
[22] K.H. Jack, Proc. R. Soc. Lond. A 208 (1951) 200. http://dx.doi.org/10.1098/rspa.1951.0154.
[23] D.H. Jack, K.H. Jack, Mater. Sci. Eng. 11 (1973) 1. http://dx.doi.org/10.1016/0025-5416(73)90055-4.
[24] M. Kopcewicz, J. Jagielski, A. Turos, D.L. Williamson, J. Appl. Phys. 71 (1992) 4217. http://dx.doi.org/10.1063/1.350801.
[25] S.J. Oh, D.C. Cook, H.E. Townsend, Hyperfine Interact. 112 (1998) 59. http://dx.doi.org/10.1023/A:1011076308501.
[26] D.M. Borsa, D.O. Boerma, Hyperfine Interact. 151/152 (2003) 31. http://dx.doi.org/10.1023/B:HYPE.0000020403.64670.02.
[27] M. Ron, A. Kidron, H. Schechter, S. Niedzwiedz, J. Appl. Phys. 18 (1967) 38. http://dx.doi.org/10.1063/1.1709379.
[28] F.E. Fujita, Metall. Trans. A 8A (1977) 1727. http://dx.doi.org/10.1007/BF02646876.
[29] L.J. Schwarzendruber, L.H. Bennett, E.A. Schoefer, W.T. Delong, H.C. Campbell, Weld. Res. Suppl. (1974) 1.
[30] Z. Cheng, C.X. Li, H. Dong, T. Bell, Surf. Coat. Technol. 191 (2005) 195. http://dx.doi.org/10.1016/j.surfcoat.2004.03.004.
[31] T. Czerwiec, H. He, G. Marcos, T. Thiriet, S. Weber, H. Michel, Plasma Process. Polym. 6 (2009) 401. http://dx.doi.org/10.1002/ppap.200930003.
[32] T.L. Christiansen, M.A.J. Somers, J. Heat Treat. Mater. 66 (2011) 2.